ACS Catalysis

Research Article

pubs.acs.org/acscatalysis

Interaction of Cobalt Nanoparticles with Oxygen- and Nitrogen-Functionalized Carbon Nanotubes and Impact on Nitrobenzene Hydrogenation Catalysis

Peirong Chen,[†] Fengkai Yang,[†] Aleksander Kostka,[‡] and Wei Xia*[,†]

[†]Laboratory of Industrial Chemistry, Ruhr-University Bochum, 44780 Bochum, Germany

[‡]Max-Planck-Institut für Eisenforschung, Max-Planck-Strasse 1, 40237 Düsseldorf, Germany

Supporting Information

ABSTRACT: The type and the amount of functional groups on the surface of carbon nanotubes (CNTs) were tuned to improve the activity of supported Co nanoparticles in hydrogenation catalysis. Surface nitrogen species on CNTs significantly promoted the decomposition of the cobalt precursor and the reduction of cobalt oxide, and improved the resistance of metallic Co against oxidation in ambient atmosphere. In the selective hydrogenation of nitrobenzene in the gas phase, Co supported on CNTs with the highest surface nitrogen content showed the highest activity, which is ascribed to the higher reducibility and the lower oxidation state of the Co nanoparticles under reaction conditions. For Co nanoparticles supported on CNTs with a smaller amount of surface nitrogen groups, a repeated reduction at 350 °C was essential to achieve a comparable high catalytic activity reaching 90% conversion at 250 °C, pointing to the importance of nitrogen species for the supported Co nanoparticles in nitrobenzene hydrogenation.

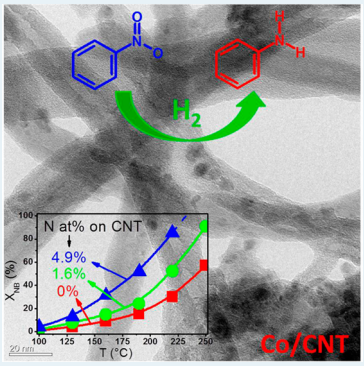

KEYWORDS: *carbon nanotubes, surface, nitrogen doping, cobalt nanoparticles, selective hydrogenation, nitrobenzene*

1. INTRODUCTION

Carbon nanotubes (CNTs) used as support for active metal nanoparticles are widely investigated in hydrogenation catalysis because of their outstanding resistance to demanding reaction conditions[1] and advantageous surface properties, which can be tuned by oxygen functionalization and nitrogen doping.[2−4] These surface functional groups can be used to tailor the catalytic performance of supported metal nanoparticles for various hydrogenation reactions.[5−9]

Nitrogen-doped carbon nanotubes (NCNTs) were found to be a promising support for hydrogenation catalysts.[6,9−11] A higher dispersion of the supported metals can be achieved on NCNTs than on nitrogen-free CNTs,[10,11] which was attributed to a higher amount of surface nucleation sites[10] and to the formation of some individual sections around the N-rich sites,[11] allowing efficient anchoring of metal nanoparticles. It was shown in our previous work[9] that Pt nanoparticles prepared by impregnation were stabilized on NCNTs against sintering in H_2 at temperatures as high as 400 °C, resulting in a smaller mean particle size as well as a narrower size distribution than on oxygen-functionalized CNTs (OCNTs). Pd nanoparticles prepared by a modified colloidal method were also found to have a narrower size distribution on NCNTs than on OCNTs.[6] These observations clearly demonstrated that NCNTs have structural beneficial effects on the supported metal nanoparticles.

In addition to the structural effect, the nitrogen functional groups on the CNT surface also showed a strong influence on the chemical state of the supported metals.[6,9,12] Supported Pd nanoparticles prepared by a modified colloidal method were found to be in a more reduced state on NCNTs than on OCNTs regardless of reduction in H_2 at 200 °C or drying in air at 60 °C, thereby pointing to the electron-donating effect of the nitrogen groups.[9] As a result of the structural and electronic-promoting effect of the NCNT support, Pd nanoparticles on NCNTs outperformed those on OCNTs with significantly higher activity and selectivity in the selective hydrogenation of cyclooctadiene (COD) to cyclooctene (COE).[9] On the contrary, supported Pt nanoparticles prepared by an impregnation method were less easily reducible as on OCNTs, presumably due to the formation of strong Pt−N bonds,[9,12] which led to a less active Pt/CNT catalyst in the hydrogenation of COD. However, the Pt nanoparticles were more selective to COE on NCNTs than on OCNTs, indicating the importance of surface nitrogen groups.[9]

Recent studies on the promoting effect of NCNT support have mainly focused on noble metals and on the comparison of oxygen and nitrogen functional groups. It is of great interest to know whether the promoting effect can be applied to non-noble metals, especially those that can be easily oxidized in air. Also, it is not clear whether the amount of nitrogen groups plays a role in hydrogenation catalysis. In this study, the type and the amount of functional groups on the surface of CNTs were tuned, aiming at tailoring the properties and catalytic

Received: October 6, 2013
Revised: March 30, 2014
Published: March 31, 2014

performance of the supported Co nanoparticles for hydrogenation catalysis. The obtained Co/CNT samples were characterized by X-ray diffraction (XRD), temperature-programmed reduction (TPR), thermogravimetry coupled with online mass spectroscopy (TG-MS), transmission electron microscopy (TEM), and X-ray photoelectron spectroscopy (XPS), and the samples were tested in the catalytic hydrogenation of nitrobenzene to aniline in the gas phase.

2. EXPERIMENTAL SECTION

2.1. Catalyst Preparation. CNTs (Baytubes C 150 P) supplied by Bayer MaterialScience (Leverkusen, Germany) were first purified by washing in diluted HNO_3 solution (1.5 mol L^{-1}) in order to remove residual catalyst used for their growth. OCNTs were prepared by treating the purified CNTs in HNO_3 vapor at 200 °C for 48 h.[2] NCNTs were synthesized either by treating the OCNTs in 10 vol % (volume percent) NH_3[3] or by feeding a nitrogen source in the CNT growth process. The obtained NCNTs were denoted as NCNT-NH_3 and NCNT-grown, respectively. Prior to any further use, NCNT-grown was purified by washing with diluted HNO_3 solution.

CNT-supported Co nanoparticles were prepared by impregnation using $Co(NO_3)_2{\cdot}6H_2O$ (Sigma-Aldrich) as precursor. Briefly, 50 mL of $Co(NO_3)_2$ aqueous solution (0.036 mol L^{-1}) and 1 g of CNTs were mixed at 30 °C for 2 h. Dark powders were obtained after removing water in a rotary evaporator, and the powders were then dried in flowing He at 120 °C for 2 h. Three different samples with the same nominal loading of 9.1 wt % (weight percent) were prepared by using three different CNT supports and designated as Co/OCNT, Co/NCNT-NH_3, and Co/NCNT-grown. The Co/CNT samples were subsequently calcined in oxygen (5 vol % O_2 in He, 100 mL min^{-1}) at 300 °C for 90 min, followed by reduction in diluted H_2 (10 vol % H_2 in He) at 350 °C for 120 min. After cooling in flowing He, the samples were slowly exposed to air.

2.2. Characterization. Inductively coupled plasma-optical emission spectroscopy (ICP-OES, PU701 UNICAM) was used to determine the Co loadings on different CNTs. XRD patterns were recorded in a Philips X'Pert MPD system with Cu Kα radiation. Scanning transmission electron microscopy (STEM) and TEM measurements were carried out with a Jeol JEM-2200FS instrument operated at 200 kV. The specimens for STEM and TEM were prepared by ultrasonically dispersing the powder samples in ethanol and dropping the suspension on a carbon-coated Au grid.

TPR experiments were preformed in a flow setup using 4.54 vol % H_2 in Ar at a flow rate of 84.1 mL min^{-1}. The TPR of the dried Co/CNT samples was performed from room temperature to 700 °C at a heating rate of 5 K min^{-1}, whereas the TPR of the calcined Co/CNT samples was performed from room temperature to 750 °C at a heating rate of 2 K min^{-1}. For each measurement, about 50 mg of Co/CNT sample was applied. The H_2 content in the evolved gases was analyzed by a thermal conductivity detector (Hydros 100, Fisher-Rosemount). TG-MS analysis was conducted in H_2 atmosphere (4.54 vol % H_2 in Ar at a flow rate of 84.1 mL min^{-1}) at a heating rate of 2 K min^{-1}. The evolved gas species were monitored by a mass spectrometer in the exhaust stream.

XPS measurements were performed in an ultrahigh vacuum setup equipped with a high-resolution Gammadata Scienta SES 2002 analyzer and a monochromatic Al Kα X-ray source (1486.6 eV, operated at 14.5 kV and 30 mA). The pressure inside the measuring chamber was kept in the range of 3.5 to 6 × 10^{-10} mbar during each measurement. The spectra were taken at a pass energy of 200 eV (high pass energy mode). Charging effects due to the insufficient conductivity of CNTs were mediated by applying a flood gun (SPECS). The CASA XPS program was employed in the analysis of XPS data. Calibration of the measured spectra was performed by positioning the C 1s peak at 284.5 eV. For the deconvolution of spectra all the parameter settings are consistent with our previous work.[3,4] Gaussian–Lorentzian mixing functions with a ratio of 70:30 and Shirley background were applied in the deconvolution of the O 1s and N 1s spectra.

2.3. Catalytic Tests. The hydrogenation of nitrobenzene (NB) is one of the most widely used approaches for the production of aniline (AN), which is an indispensible raw material in the production of methylene diphenyl diisocyanate. The proposed reaction pathway of NB hydrogenation is shown in Scheme 1. Nitrobenzene can be partially hydrogenated to nitrosobenzene (NSB) and fully hydrogenated to AN.

Scheme 1. Reaction Pathway of Nitrobenzene Hydrogenation

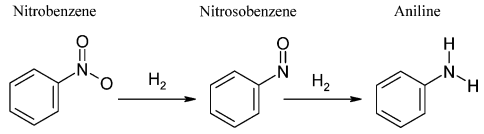

NB hydrogenation was performed in the gas phase in a fixed-bed reactor under plug-flow conditions. A constant nitrobenzene flow was obtained by passing He through liquid NB at 70 °C. The composition of the gas feed with a total flow rate of 100 mL min^{-1} was 0.3 vol % NB, 3.0 vol % H_2, and 96.7 vol % He. One hundred milligrams of the calcined Co/CNT catalysts were loaded into the glass reactor. The reactants and products were monitored by an online gas chromatograph (Shimadzu GC-2014) equipped with a flame ionization detector, a HP-5 capillary column, and a Valco sample loop. A control experiment without any catalyst was performed prior to the catalytic tests, and conversion of NB was not detected under applied conditions.

The reduction of the Co/CNT catalysts was carried out in diluted H_2 (10 vol % H_2 in He) at 350 °C for 2 h prior to each catalytic test. The activity of the reduced Co/CNT samples was evaluated at six different temperatures in the range of 100 to 250 °C. In order to achieve steady-state conditions, the reaction was performed for 1 h at each temperature, and then the NB conversion was recorded and used for activity evaluation. The catalytic activities of the used Co/CNT catalysts were re-examined after a repeated reduction in H_2 at 350 °C for 2 h. Reference tests using OCNT, NCNT-NH_3, and NCNT-grown as catalysts without Co were conducted as well for comparison. The conversion of NB (X_{NB}) and the selectivity to AN (S_{AN}) and NSB (S_{NSB}) were calculated according to eqs 1, 2, and 3, respectively.

$$X_{NB} = \frac{C_{NB,0} - C_{NB}}{C_{NB,0}} \times 100\% \quad (1)$$

$$S_{AN} = \frac{C_{AN}}{C_{NB,0} - C_{NB}} \times 100\% \quad (2)$$

$$S_{NSB} = \frac{C_{NSB}}{C_{NB,0} - C_{NB}} \times 100\% \quad (3)$$

In the equations, $C_{NB,0}$ is the initial NB concentration in the gas feed, C_{NB}, C_{AN}, and C_{NSB} are the concentrations of NB, AN, and NSB monitored by the online GC during the hydrogenation reaction. A carbon balance of 100 ± 6% was achieved in all the tests.

3. RESULTS AND DISCUSSION

3.1. Characterization of the CNT Supports and Co/CNT Catalysts. All the CNTs were synthesized using the same growth catalyst and show similar outer diameters. A detailed description of OCNT and NCNT-NH_3 can be found elsewhere.[6,9,13] Physisorption studies of N_2 show similar type of isotherms and pore size distributions despite differences in the specific surface area of the three types of CNTs used in this study (Table S1, Figure S1). The main difference among them is the surface chemistry. Surface characterization by XPS revealed that there are very different types and amounts of surface functional groups (Table S1, refs 6 and 9). Plenty of

dx.doi.org/10.1021/cs500173t | ACS Catal. 2014, 4, 1478–1486

surface defects were detected by Raman analysis (Figure S2). It is believed that the surface chemistry, including functional groups and defects, can significantly influence supported metal nanoparticles.[6,9,14,15] Residual growth catalysts (Co, Mn, Mg, and Al) were detected by ICP-OES (Table S2) but not visible in XPS (Figure S3), indicating the absence of residual metal species on the CNT surface after purification.[9] Therefore, catalytic contribution of the residual growth catalyst in hydrogenation catalysis can be excluded.[13]

The OCNT, NCNT-NH_3, and NCNT-grown samples were then used as supports for Co nanoparticles resulting in three Co/CNT catalysts. The achieved Co weight loadings were determined by ICP-OES to be 6.98%, 7.01% and 7.23% for Co/OCNT, Co/NCNT-NH_3, and Co/NCNT-grown, respectively. The slightly higher Co loading on NCNT-grown is likely due to a larger amount of nitrogen groups acting as strong anchoring sites for Co species.[6,10]

After impregnation, the obtained Co/CNT samples were dried in He at 120 °C, calcined in air at 300 °C, and subsequently reduced in H_2 at 350 °C. XRD analysis was performed after each treatment step. It has to be noted that in the whole procedure, the Co/CNT samples were transferred in air, and cobalt oxides were supposed to form upon contact with air even for the reduced Co/CNT samples. The XRD patterns of the Co/CNT samples after drying in flowing He at 120 °C are displayed in Figure 1a. Reflections at around 26° and 42.4° were observed in all the three samples, which can be attributed to the (002) and (111) planes of the hexagonal graphite structure of CNTs, respectively. In addition, peaks at 18.9°, 31.3°, 36.8°, 44.8°, 59.3°, and 65.2° were recorded, which are the characteristic (111), (220), (311), (400), (511), and (440) reflections of Co_3O_4 (PDF 42-1467), respectively. The diffraction peaks are broader with lower intensities for Co on OCNTs, whereas the intensities of Co_3O_4 are stronger on NCNT-NH_3. Even stronger reflections were observed for Co on NCNT-grown, indicating the presence of a larger amount of crystalline Co_3O_4.

The dried Co/CNT samples were calcined in air at 300 °C, and their XRD patterns are shown in Figure 1b. As expected, intense Co_3O_4 diffractions were observed for all the three samples without a significant difference. The calcined Co/CNT samples were subsequently reduced in H_2 at 350 °C, as suggested in the literature.[16] The diffraction patterns of the reduced samples are shown in Figure 1c. It can be seen that the reduced Co/OCNT sample shows a very similar diffraction pattern as after calcination, which can be related to the incomplete reduction of Co_3O_4 and/or the fast reoxidation of reduced Co on OCNTs due to the exposure to air. Interestingly, as compared to the reduced Co/OCNT sample, the diffraction pattern resulting from Co_3O_4 is much weaker for the reduced Co/NCNT-NH_3 sample, indicating a more complete reduction of Co_3O_4 and/or less severe reoxidation of the reduced Co on NCNT-NH_3. The weakest Co_3O_4 reflections were observed for Co/NCNT-grown among the three reduced Co/CNT samples. Instead, a strong peak due to the (111) reflection of cubic Co (PDF 15-0806) was recorded at ca. 44.5°. As demonstrated by the reflections in the range between 40 and 50°, a clear decrease of the Co_3O_4 intensity and an increase in metallic Co intensity occurred due to the increase in nitrogen content from 0 to 4.9 at. % (atomic percent) on the CNT surface (insert in Figure 1c). The XRD results revealed that the surface chemistry of the CNT supports had significant impacts on the composition and structure of

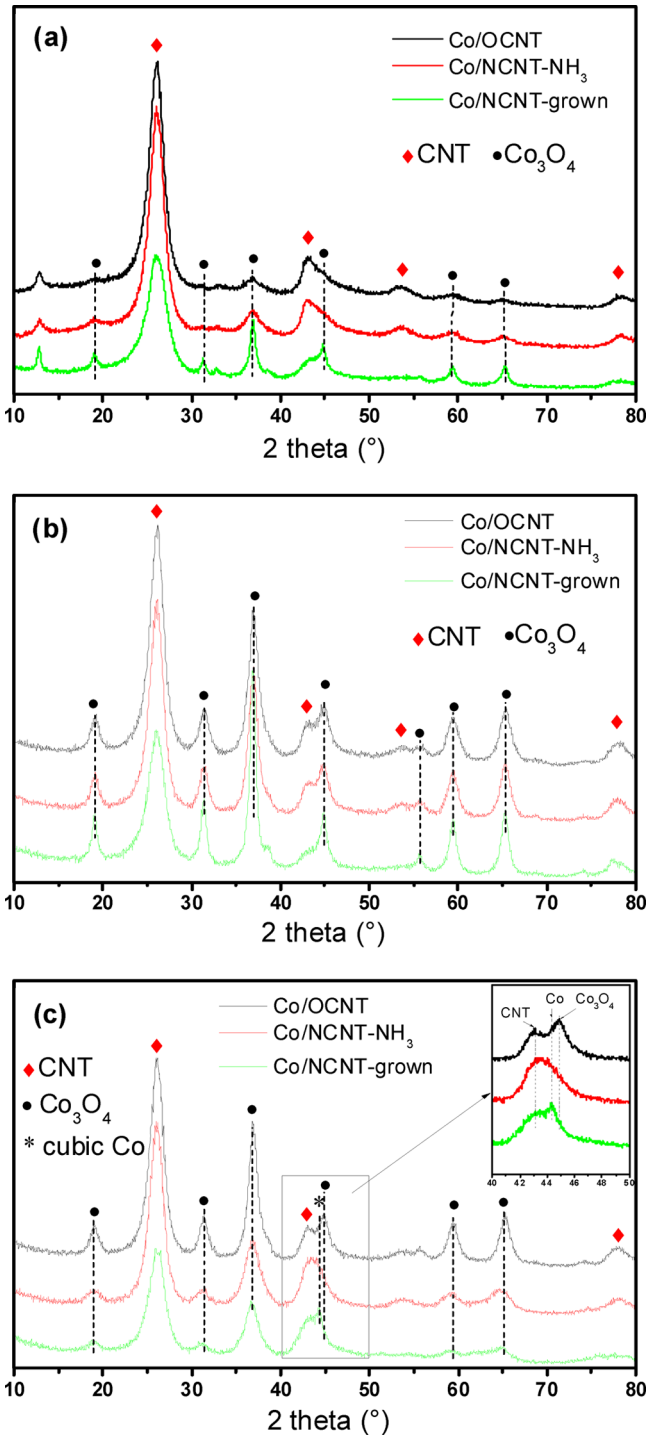

Figure 1. XRD patterns of the Co/CNT samples after drying in He at 120 °C (a), after calcination in air at 300 °C (b), and after reduction in H_2 at 350 °C (c). All the samples were transferred in air for the XRD analysis.

prepared Co/CNT samples during both the drying in He and the reduction in H_2.

The influence of the CNT supports on the reduction behavior of the supported Co was investigated by TPR studies. The obtained H_2 uptake profiles of the dried and the calcined Co/CNT samples are displayed in Figure 2a,b, respectively. Two peaks were observed at temperatures lower than 300 °C in the TPR profiles of the three dried samples (Figure 2a). The

dx.doi.org/10.1021/cs500173t | ACS Catal. 2014, 4, 1478−1486

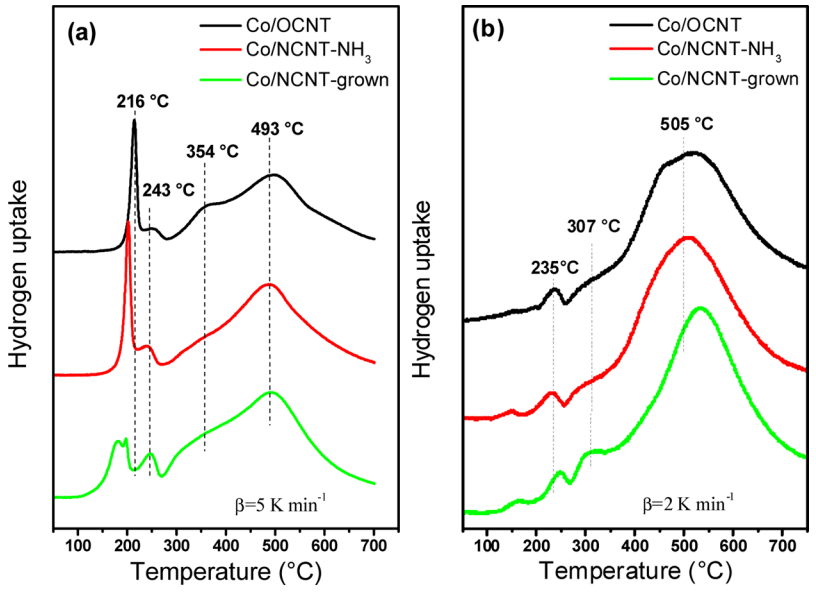

Figure 2. TPR profiles of Co/CNT samples after drying in flowing He at 120 °C (a) and after calcination in air at 300 °C (b).

major peak is related to the decomposition of the cobalt nitrate precursor, as described in eqs 4 and 5:[17]

$$2Co(NO_3)_2 \rightarrow Co_2O_3 + N_2O_4 + N_2O_5 \quad (4)$$

$$3Co(NO_3)_2 \rightarrow Co_3O_4 + N_2O_4 + 2N_2O_5 \quad (5)$$

The major peaks for Co/OCNT and Co/NCNT-NH_3 are very similar in terms of peak shape and peak intensity. However, the position of the major peak for Co/NCNT-NH_3 was shifted to a lower temperature of ca. 205 °C, as compared to ca. 220 °C for Co/OCNT, indicating the promoting effect of the surface nitrogen on the decomposition of cobalt nitrate. For the sample Co/NCNT-grown, a broad decomposition peak centered at ca. 180 °C was recorded in the TPR profile, which can be related to a stronger promoting effect from the increased N concentration on the CNT surface. A minor peak centered at ca. 240 °C was found in the three TPR profiles due to the reduction of the cobalt oxides (formed through precursor decomposition) to CoO.[18] A shoulder in the temperature range from 300 to 355 °C was observed as well in each TPR profile, which is attributed to the reduction of CoO to metallic Co.[19] This two-step reduction of Co_3O_4 or Co_2O_3 to metallic Co was following the route shown in eq 6 and has been analyzed in depth in the literature.[19,20] The H_2 consumption peak centered at ca. 500 °C (Figure 2a) is related to the reduction of the surface oxygen groups and the gasification of the CNT support,[4,19] which is confirmed by a comparative TPR study over pure OCNT support without supported Co (Figure S4).

$$Co_3O_4/Co_2O_3 \rightarrow CoO \rightarrow Co \quad (6)$$

In the TPR of the calcined Co/CNT samples, a lower heating ramp of 2 K min^{-1} was applied in order to distinguish the exact reduction temperature of different species, and very different reduction behaviors were observed, as shown in Figure 2b. A clear peak at ca. 235 °C was observed in all the three samples due to the reduction of Co_3O_4 to CoO.[19] The reduction of CoO to metallic Co starting at ca. 260 °C led to a clearly visible H_2 uptake peak at ca. 307 °C in the TPR profile of Co/NCNT-grown, but only to broad shoulders in the TPR profiles of Co/OCNT and Co/NCNT-NH_3.[19] The enhanced reduction of cationic Co on NCNT-grown clearly indicates that the surface N species can promote the reduction of cobalt oxides on CNTs. The electron-donating effect of surface N species, as observed in several previous studies,[6,21,22] is assumed to be responsible for the promoting effect. Besides, the metal cations were believed to be preferably located on N-containing sites on the carbon surface,[23] which possess modified local electronic structure likely favoring the reduction of supported Co.[15] In case of NCNT-grown with a higher surface N content, the local electronic structure can be more significantly modified,[24] leading to a more pronounced promoting effect.

The reduction process was repeated using TG-MS analysis under similar conditions as those applied in the TPR experiments, and the results are shown in Figure 3. It can be

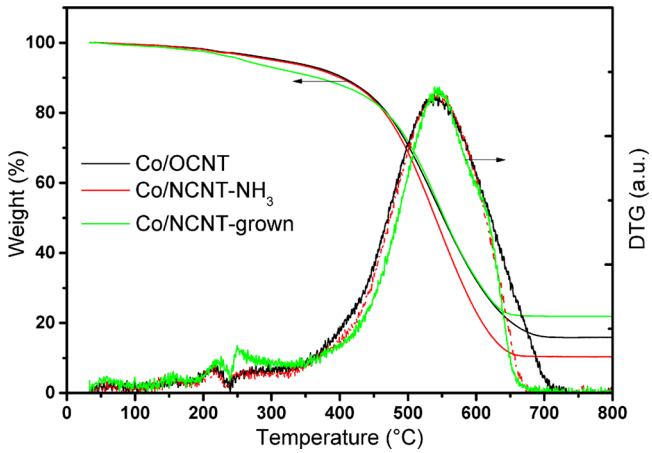

Figure 3. TG-DTG curves of Co/CNT samples heated in H_2 (4.54 vol % H_2 in He) using a heating ramp of 2 K min^{-1}.

seen from the TG-DTG curves (Figure 3) that there is a slight weight loss at temperatures lower than 400 °C due to the thermal removal of adsorbed water, the reductive removal of surface oxygen, and the reduction of cobalt oxide to metallic Co. A clear peak at ca. 230 °C was observed in all three DTG curves, corresponding to the reduction of Co_3O_4 to CoO

dx.doi.org/10.1021/cs500173t | ACS Catal. 2014, 4, 1478−1486

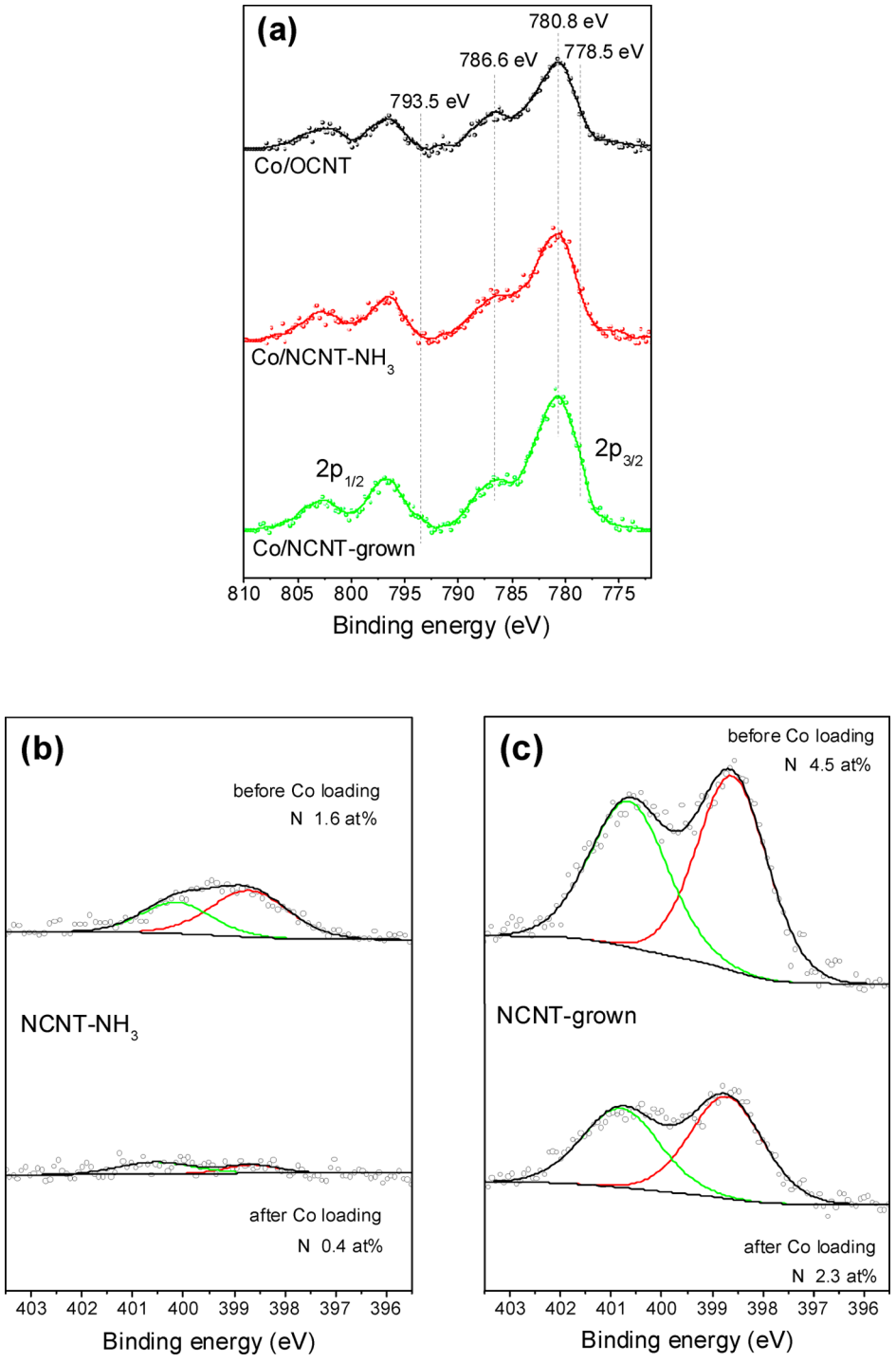

Figure 4. XPS studies. (a) Co 2p spectra of the Co/CNT samples after reduction; (b) N 1s spectra of NCNT-NH_3 before and after Co loading; (c) N 1s spectra of NCNT-grown before and after Co loading. The spectra were normalized, and the N 1s spectra are plotted using the same scale for comparison.

(Figure 2b), whereas the increased DTG intensity starting at ca. 260 °C is related to the reduction of CoO to metallic Co corresponding to the increased H_2 consumption in the TPR profiles appearing at the same temperatures. The clearly higher DTG intensity of Co/NCNT-grown in the temperature range from 260 to 320 °C is in agreement with the H_2 uptake peak at ca. 307 °C in the TPR profile of Co/NCNT-grown. Gasification of CNTs was found to start at ca. 350 °C and to be accelerated beyond 400 °C, yielding methane as indicated by the MS signal with m/z = 16 and m/z = 14 (not shown), which is consistent with literature results.[19] The TG-MS results imply that it is important to keep the temperature below 350 °C in the reduction of cobalt oxide supported on CNTs.

It is worth noting that the residual weights after TG analysis (Figure 3) are very different for the three Co/CNT samples. As shown in previous work,[9] OCNT and NCNT-NH_3 were prepared using purified CNTs and have a very small amount (less than 0.15 wt %, see Table S2) of residual growth catalyst. Hence, the higher residual weight of Co/OCNT compared with Co/NCNT-NH_3 can be ascribed to the formation of

dx.doi.org/10.1021/cs500173t | ACS Catal. 2014, 4, 1478−1486

cobalt carbide,[25,26] which is difficult to remove in reducing atmosphere. The highest residual weight was observed for the Co/NCNT-grown sample, which is related to a higher amount of residual growth catalyst even after purification and the formation of cobalt carbide or cobalt nitride.[25−27]

The surface chemistry of the Co/CNT samples after reduction at 350 °C was examined using XPS. The observed Co 2p spectra are shown in Figure 4a. The main Co $2p_{3/2}$ peaks for all the three samples were found to be at 780.8 eV revealing that Co is mainly in the oxidized state, which is related to the reoxidation of the reduced Co during the transfer in air. The characteristic shakeup peak of CoO at 786.6 eV was recorded in all the three samples,[28−30] indicating the presence of a large portion of CoO in the investigated samples. In the case of Co/NCNT-grown, a minor contribution was recorded at a lower binding energy of 778.5 eV leading to a shoulder in the spectrum, which can be assigned to Co in the metallic state. A corresponding contribution resulting from metallic Co was observed as well at 793.5 eV in the Co $2p_{1/2}$ region. The presence of metallic Co confirms the stabilization effect of the NCNT support as revealed by the XRD analysis. It has to be noted that XPS is highly surface-sensitive, and the probing depth is only limited to a few nanometers. Therefore, the signal from metallic Co is much weaker than that observed in XRD due to the formation of a cobalt oxide layer on the outer surface of the Co nanoparticles after exposure to air.

The loading of Co nanoparticles modified the surface composition of CNT supports, especially the surface N species (Figure 4b,c). Both pyridinic (at ca. 398.5 eV) and pyrrolic (at ca. 400.5 eV) N groups were detected on NCNT supports before and after Co loading.[6,9] Quantitative XPS analysis demonstrated that the total amount (atomic percentage) of surface N species significantly decreased on both NCNT-NH_3 and NCNT-grown after Co deposition, which can be attributed to the coverage of N groups serving as strong anchoring sites by the anchored Co nanoparticles.[6] Comparing the deconvoluted XP N 1s spectra before and after Co loading, we cannot observe clear preferential anchoring of Co on certain N species (Figure 4b,c), which is in agreement with our previous observations.[6] Although there is clear evidence of the interaction between metal particles and nitrogen species on NCNTs,[6,9,15,22,31] it is practically very challenging to establish a precise correlation between certain nitrogen species and the properties of the supported metal nanoparticles. One of the major obstacles is the controlled synthesis of certain nitrogen groups. Nearly all the syntheses of NCNTs so far lead to a mixture of different surface N groups. Moreover, the N groups are often not uniformly but rather shape-selectively distributed on CNTs.[24,32] All these problems complicated the metal−NCNT system and consequently hindered the full understanding of metal−N interactions.

3.2. Catalytic Hydrogenation of Nitrobenzene Using Co/CNT as Catalysts. The intrinsic activities of the catalyst supports (i.e., OCNT, NCNT-NH_3, and NCNT-grown) were first examined as reference in the selective hydrogenation of NB at different temperatures in the range of 100−250 °C, and the observed NB conversions are displayed in Figure 5a as a function of reaction temperature. It can be seen that both OCNT and NCNT-NH_3 show almost no activity in NB hydrogenation even at a high reaction temperature of 250 °C, whereas considerable NB conversion was achieved over NCNT-grown at all reaction temperatures. The presence of a larger amount of nitrogen-containing sites that are active in

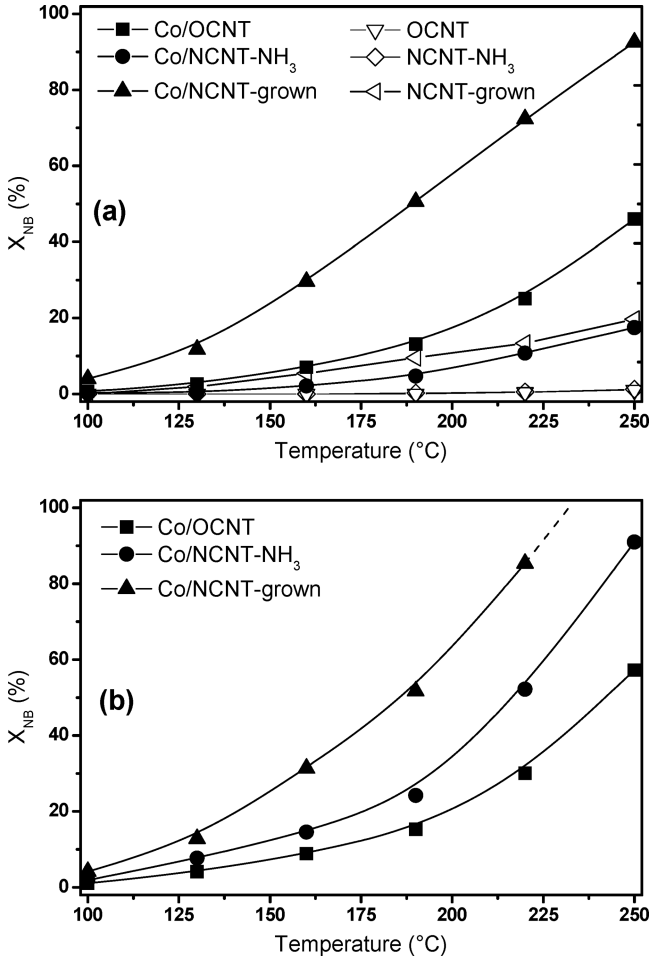

Figure 5. Nitrobenzene conversion (X_{NB}) as a function of reaction temperature in the selective hydrogenation of nitrobenzene using (a) freshly reduced Co/CNT catalysts and (b) Co/CNT catalysts after one run of reaction and second reduction. The intrinsic activities of the CNT supports are shown as reference. Extrapolation of the conversion−temperature curve (dashed line in Figure 5b) was performed for the repeatedly reduced Co/NCNT-grown catalyst to estimate the lowest temperature reaching full conversion of NB. Reduction at 350 °C was performed prior to the catalytic test in both runs.

hydrogenation catalysis is assumed to be the reason.[13] Residual growth catalyst in NCNT-grown, despite its higher amount than that in OCNT or NCNT-NH_3, has no detectable contribution in gas phase hydrogenation reactions due to encapsulation and absence from the surface (see XPS in Figure S3).[13] However, it has to be noted that in electrocatalysis carried out in liquid phase, even traces of residual growth catalyst could significantly influence the electrocatalytic performance of NCNTs.[33]

The hydrogenation activities of the three freshly reduced Co/CNT catalysts were tested following the same procedure as for the CNT supports. A repeated hydrogenation test was conducted for each used Co/CNT catalyst after a repeated reduction at 350 °C. The results of the first and the second run are shown in Figure 5a,b, respectively.

In both runs, NB conversion over all the three catalysts was found to increase with increasing reaction temperatures. In the first run using freshly reduced Co/CNT catalysts, a significantly higher degree of NB conversion was achieved over Co/NCNT-

dx.doi.org/10.1021/cs500173t | ACS Catal. 2014, 4, 1478−1486

grown as compared to Co/OCNT and Co/NCNT-NH_3 at each chosen reaction temperature. The promoting effect of the NCNT-grown support leading to more reduced Co nanoparticles is assumed to be responsible for the higher NB conversion of Co/NCNT-grown. However, minor contributions from the higher Co loading and the higher amount of surface nitrogen cannot be completely excluded. Using Co/NCNT-grown as catalyst, a rapid increase in NB conversion was observed with increasing reaction temperatures, and a NB conversion higher than 90% was obtained at 250 °C. Surprisingly, the activity of Co/NCNT-NH_3 is lower than that of Co/OCNT at the same reaction temperature.

At each reaction temperature, the Co/NCNT-grown catalyst showed a slightly higher degree of NB conversion in the second run than in the first run, and the full conversion of NB was estimated to be achieved at ca. 230 °C (Figure 5b). A very slight increase in NB conversion occurred as well in the case of Co/OCNT. Interestingly, Co/NCNT-NH_3 showed a significantly higher NB conversion in the second run than in the first run and reached 90% conversion at the reaction temperature of 250 °C. The slightly increased activity of Co/OCNT and Co/NCNT-grown is probably due to the more reduced Co nanoparticles after the repeated reduction. For Co/NCNT-NH_3, an enhanced interaction between Co and the NCNT-NH_3 support resulting from the repeated reduction is assumed to be responsible for the significantly increased activity in the second run.[6] The comparison of the three Co/CNT catalysts indicates that a high nitrogen content on CNT surface is of great importance to achieve durable high performance in this reaction, whereas a more complete reduction is required for Co supported on CNTs with a low nitrogen content to achieve a comparable activity. All the three Co/CNT catalysts showed a high selectivity to aniline amounting to more than 95% in both runs without distinguishable differences, indicating that the Co/CNT samples are promising catalysts in selective hydrogenation of NB. The specific activity, that is, the amount of converted NB normalized by the total amount of Co on each CNT support, demonstrated similar trend in both runs (Figure S5). Specifically, Co/NCNT-grown was the most active in both runs in terms of specific activity, whereas the specific activity of Co/NCNT-NH_3 was significantly improved in the second run. This observation implies that the Co loading is not a decisive factor in this reaction.

To investigate the influence of reduction time, Co/NCNT-NH_3 and Co/NCNT-grown catalysts reduced for a longer time of 4 h were tested (Figure S6). For Co/NCNT-NH_3, an activity higher than the first run but less than the second run was achieved, which can be related to the intermediate reduction degree of Co. Note that Co in the second run was more deeply reduced because of the reduction during the first run of reaction. On the contrary, Co/NCNT-grown reduced for 4 h showed a similar activity as that in the first and second runs, indicating that Co was nearly fully reduced after reduction for 2 h. On the one hand, more metallic Co sites were generated as a result of the promoting effect of N groups on the surface of NCNT-grown, leading to more efficient activation and dissociation of H_2 and nitrobenzene.[6] On the other hand, CoN_x species that are highly active in the hydrogenation of nitroarenes[34] can be more easily formed on NCNT-grown because of the close contact between the metal cations and N-containing sites on carbon surface.[23] As a consequence, higher hydrogenation activity was achieved on NCNTs with a higher amount of surface N groups. This result is in good agreement with our previous work using Pd as active phase for hydrogenation.[6] Nevertheless, more mechanistic investigations using in situ techniques are required to gain a deeper insight into the promoting effect of NCNTs.

The catalytic stability of the Co/CNT catalysts was tested at 250 °C for 3 h, during which the catalysts showed no signs of deactivation (Figure S7). In all the above-mentioned catalytic tests, NSB was detected to be the only byproduct, confirming the reaction pathway proposed in Scheme 1. The formation of polymerized products was not observed in the system after long time operation. The outstanding catalytic performance points to the high potential of the synthesized Co/CNT catalysts in industrial-related applications.

3.3. Characterization of Co/CNT after Hydrogenation Reactions. XRD investigations were performed with the Co/CNT catalysts after the hydrogenation tests, and the results are displayed in Figure 6. CoO rather than Co_3O_4 was found to be

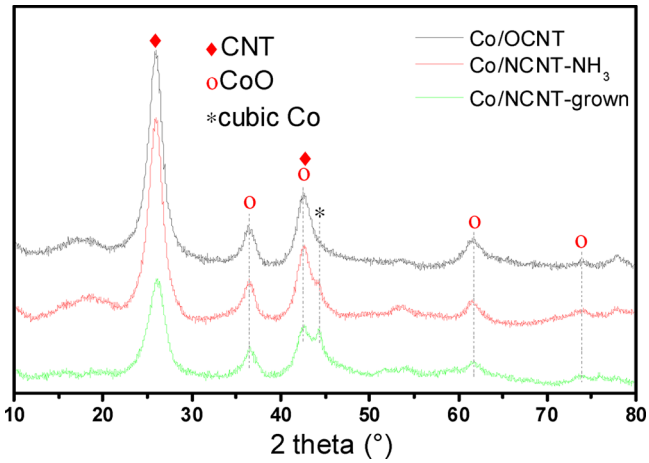

Figure 6. XRD patterns of the Co/CNT samples after two hydrogenation runs. All the samples were transferred in air for the XRD analysis.

the main oxide phase, obviously due to the reoxidation of metallic Co upon contact with air. Very clear cubic Co reflections were recorded for Co supported on NCNT-NH_3 and NCNT-grown after the hydrogenation reactions, confirming the improved resistance of metallic Co against oxidation in ambient atmosphere. A stronger cubic Co signal was observed on NCNT-grown demonstrating the relevance of a higher content of surface nitrogen. It has to be pointed out that cobalt carbide and cobalt nitride may form as well during the reduction process.[35−37] However, they cannot be clearly distinguished by XRD, because their main diffraction peak at around 44.5° is very close to that of the cubic Co.

Figure 7 shows representative STEM and TEM images and the corresponding particle size distributions of the Co/CNT catalysts after the hydrogenation tests. Highly dispersed Co nanoparticles smaller than 10 nm were observed on all the three CNT supports (Figure 7a,d,g). However, on OCNT and NCNT-NH_3 supports, large Co particles can always be found, whereas the particle size on NCNT-grown seems to be more uniform, and large particles were seldom detected. The TEM images show that the Co nanoparticles in all the three catalysts are located on the outer surface of the CNTs. Statistical analysis of the particle size was carried out by measuring the size of ca. 100 Co nanoparticles, which yielded the histograms shown in Figure 7j–l. It can be seen that the average particle size of Co

dx.doi.org/10.1021/cs500173t | ACS Catal. 2014, 4, 1478−1486

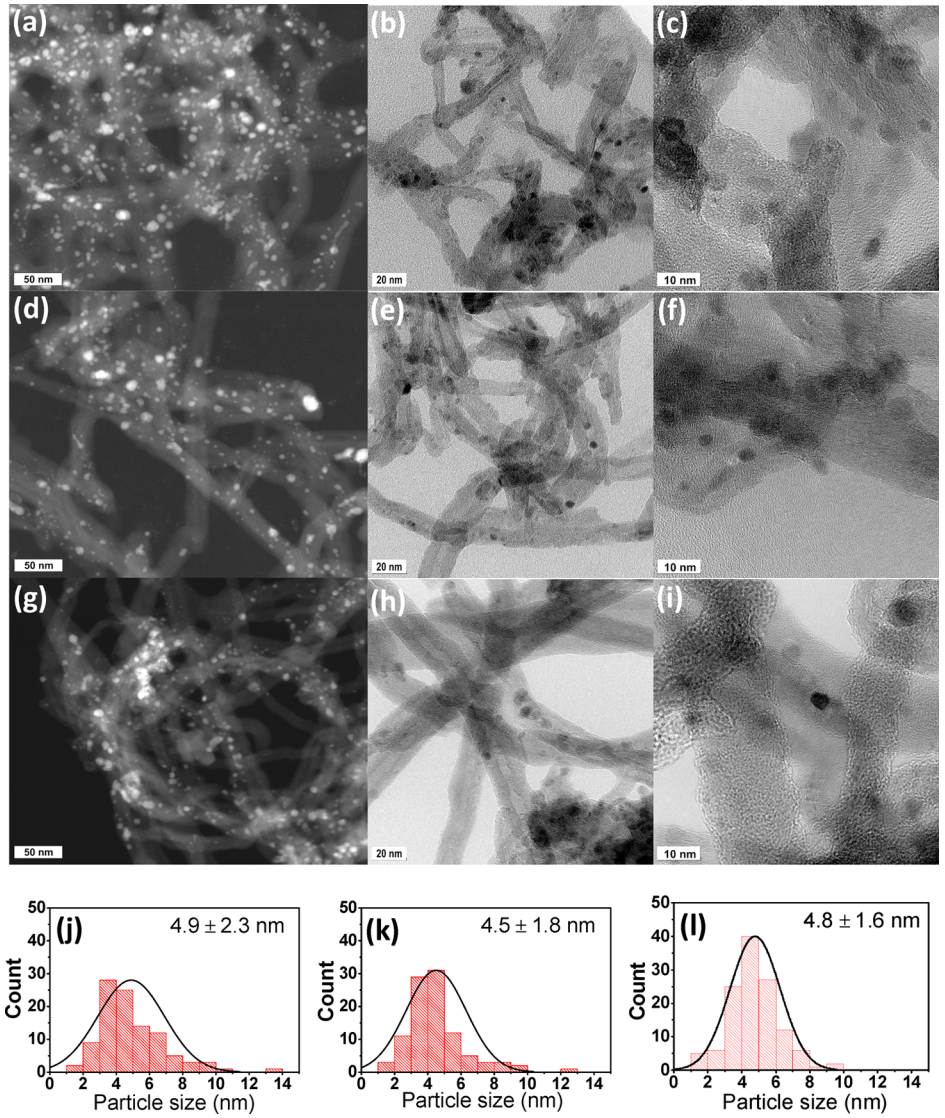

Figure 7. Representative STEM and TEM images of Co/OCNT (a–c), Co/NCNT-NH_3 (d–f) and Co/NCNT-grown (g–i); particle size distributions of Co/OCNT (j), Co/NCNT-NH_3 (k), and Co/NCNT-grown (l) obtained by measuring ca. 100 particles. The Co/CNT samples were analyzed after the hydrogenation tests.

nanoparticles is in the range of 4.5–4.9 nm without substantial differences on the three CNT supports. The particle size of Co on carbon support is often related to the metal loading, that is, a higher Co loading usually leads to larger Co particles.[38] In case of Co/NCNT-grown, the size of Co nanoparticles remains small despite a higher Co loading, which can be attributed to the strong anchoring effect of surface N groups in accordance with our previous observations.[6,9] Furthermore, the particle size distribution of Co nanoparticles, as indicated by the histograms and the deviations of the average particle size, is slightly narrower on NCNTs than on OCNT due to the stabilizing effect from the nitrogen groups on CNT surface.[6,9] It is noteworthy that the difference with respect to the particle size distribution is much smaller in the present Co/CNT system with 7–8 wt % Co than in the low-loaded Pt/CNT[9] and Pd/CNT[6] systems, likely due to the limited influence of nitrogen groups in the case of a much higher metal loading.

4. CONCLUSIONS

On the CNT surface, both the decomposition of the cobalt precursor and the reduction of the cobalt oxides were significantly promoted by surface nitrogen species. Clearly improved resistance against oxidation in ambient atmosphere was achieved for metallic Co supported on directly grown NCNTs (NCNT-grown) with a large amount of surface nitrogen. The supported Co nanoparticles were found to have a narrower size distribution on NCNTs than on OCNTs. In the selective hydrogenation of nitrobenzene, a very high selectivity to aniline was achieved over all the three Co/CNT catalysts. Freshly reduced Co nanoparticles on NCNT-grown showed the highest activity reaching more than 90% conversion at 250 °C, which can be assigned to a more complete reduction and a lower oxidation state of Co under reaction conditions due to the promotion effect of nitrogen species on the support. After a repeated reduction, the activity of Co on NCNT-NH_3 was significantly enhanced leading to 90% conversion at 250 °C. Thus, a highly active and stable hydrogenation catalyst can be obtained by supporting Co nanoparticles on CNTs with high

dx.doi.org/10.1021/cs500173t | ACS Catal. 2014, 4, 1478–1486

surface nitrogen content, suggesting a new route for the preparation of high-performance catalysts by tuning the surface properties of the CNT support.

■ ASSOCIATED CONTENT

Supporting Information

Characterizations of the CNT supports by nitrogen physisorption, Raman, and XPS; further catalytic tests. This material is available free of charge via the Internet at http://pubs.acs.org/.

■ AUTHOR INFORMATION

Corresponding Author

*E-mail: wei.xia@techem.rub.de. Fax: +49 234 32 14115. Tel.: +49 234 32 22341.

Notes

The authors declare no competing financial interest.

■ ACKNOWLEDGMENTS

Financial support from the German Federal Ministry of Education and Research (BMBF) for the CarboKat project (03X0204D) within the scope of the Inno.CNT Alliance is gratefully acknowledged. The authors thank Martin Muhler for fruitful discussion.

■ REFERENCES

(1) Oosthuizen, R. S.; Nyamori, V. O. *Platinum Met. Rev.* **2011**, *55*, 154−169.
(2) Xia, W.; Jin, C.; Kundu, S.; Muhler, M. *Carbon* **2009**, *47*, 919−922.
(3) Kundu, S.; Xia, W.; Busser, W.; Becker, M.; Schmidt, D. A.; Havenith, M.; Muhler, M. *Phys. Chem. Chem. Phys.* **2010**, *12*, 4351−4359.
(4) Kundu, S.; Wang, Y.; Xia, W.; Muhler, M. *J. Phys. Chem. C* **2008**, *112*, 16869−16878.
(5) Sahin, S.; Mäki-Arvela, P.; Tessonnier, J. P.; Villa, A.; Reiche, S.; Wrabetz, S.; Su, D. S.; Schlögl, R.; Salmi, T.; Murzin, D. Y. *Appl. Catal. A: Gen.* **2011**, *408*, 137−147.
(6) Chen, P.; Chew, L.; Kostka, A.; Muhler, M.; Xia, W. *Catal. Sci. Technol.* **2013**, *3*, 1964−1971.
(7) Xia, W.; Schlüter, O. F. K.; Liang, C.; van den Berg, M. W.; Guraya, M.; Muhler, M. *Catal. Today* **2005**, *102−103*, 34−39.
(8) Zgolicz, P. D.; Stassi, J. P.; Yañez, M. J.; Scelza, O. A.; Miguel, S. R. *J. Catal.* **2012**, *290*, 37−54.
(9) Chen, P.; Chew, L.; Xia, W. *J. Catal.* **2013**, *307*, 84−93.
(10) Chizari, K.; Janowska, I.; Houllé, M.; Florea, I.; Ersen, O.; Romero, T.; Bernhardt, P.; Ledoux, M. J.; Pham-Huu, C. *Appl. Catal. A: Gen.* **2010**, *380*, 72−80.
(11) Lepró, X.; Terrés, E.; Vega-Cantú, Y.; Rodríguez-Macías, F. J.; Muramatsu, H.; Kim, Y. A.; Hayahsi, T.; Endo, M.; Torres, M.; Terrones, M. *Chem. Phys. Lett.* **2008**, *463*, 124−129.
(12) Sun, C. L.; Pao, C. W.; Tsai, H. M.; Chiou, J. W.; Ray, S. C.; Wang, H. W.; Hayashi, M.; Chen, L. C.; Lin, H. J.; Lee, J. F.; Chang, L.; Tsai, M. H.; Chen, K. H.; Pong, W. F. *Nanoscale* **2013**, *5*, 6812−6818.
(13) Chen, P.; Chew, L.; Kostka, A.; Xie, K.; Muhler, M.; Xia, W. *J. Energy Chem.* **2013**, *22*, 312−320.
(14) Shao, L.; Zhang, B.; Zhang, W.; Hong, S. Y.; Schlögl, R.; Su, D. S. *Angew. Chem., Int. Ed.* **2013**, *52*, 2114−2117.
(15) Arrigo, R.; Schuster, M. E.; Abate, S.; Wrabetz, S.; Amakawa, K.; Teschner, D.; Freni, M.; Centi, G.; Perathoner, S.; Havecker, M.; Schlögl, R. *ChemSusChem* **2014**, *7*, 179−194.
(16) Bezemer, G. L.; Bitter, J. H.; Kuipers, H. P.; Oosterbeek, H.; Holewijn, J. E.; Xu, X.; Kapteijn, F.; van Dillen, A. J.; de Jong, K. P. *J. Am. Chem. Soc.* **2006**, *128*, 3956−3964.
(17) Ehrhardt, C.; Gjikaj, M.; Brockner, W. *Thermochim. Acta* **2005**, *432*, 36−40.
(18) Sewell, G. S.; Steen, E.; O'Connor, C. T. *Catal. Lett.* **1996**, *37*, 255−260.
(19) Bezemer, G. L.; Radkevich, V.; Falke, U.; Oosterbeek, H.; Kuipers, H.; Vandillen, A.; de Jong, K. P. *J. Catal.* **2006**, *237*, 152−161.
(20) Becker, M.; Xia, W.; Tessonnier, J. P.; Blume, R.; Yao, L.; Schlögl, R.; Muhler, M. *Carbon* **2011**, *49*, 5253−5264.
(21) Arrigo, R.; Havecker, M.; Wrabetz, S.; Blume, R.; Lerch, M.; McGregor, J.; Parrott, E. P.; Zeitler, J. A.; Gladden, L. F.; Knop-Gericke, A.; Schlögl, R.; Su, D. S. *J. Am. Chem. Soc.* **2010**, *132*, 9616−9630.
(22) Arrigo, R.; Wrabetz, S.; Schuster, M. E.; Wang, D.; Villa, A.; Rosenthal, D.; Girsgdies, F.; Weinberg, G.; Prati, L.; Schlögl, R.; Su, D. S. *Phys. Chem. Chem. Phys.* **2012**, *14*, 10523−10532.
(23) Pylypenko, S.; Borisevich, A.; More, K. L.; Corpuz, A. R.; Holme, T.; Dameron, A. A.; Olson, T. S.; Dinh, H. N.; Gennett, T.; O'Hayre, R. *Energy Environ. Sci.* **2013**, *6*, 2957−2964.
(24) Florea, I.; Ersen, O.; Arenal, R.; Ihiawakrim, D.; Messaoudi, C.; Chizari, K.; Janowska, I.; Pham-Huu, C. *J. Am. Chem. Soc.* **2012**, *134*, 9672−9680.
(25) Cheng, J.; Hu, P.; Ellis, P.; French, S.; Kelly, G.; Lok, C. M. *J. Phys. Chem. C* **2010**, *114*, 1085−1093.
(26) Karaca, H.; Safonova, O. V.; Chambrey, S.; Fongarland, P.; Roussel, P.; Griboval-Constant, A.; Lacroix, M.; Khodakov, A. Y. *J. Catal.* **2011**, *277*, 14−26.
(27) van Dommele, S.; Romero-Izquirdo, A.; Brydson, R.; de Jong, K. P.; Bitter, J. *Carbon* **2008**, *46*, 138−148.
(28) Biesinger, M. C.; Payne, B. P.; Grosvenor, A. P.; Lau, L. W.; Gerson, A. R.; Smart, R. S. *Appl. Surf. Sci.* **2011**, *257*, 2717−2730.
(29) Voß, M.; Borgmann, D.; Wedler, G. *J. Catal.* **2002**, *212*, 10−21.
(30) Zhang, L.; Dong, L.; Yu, W.; Liu, L.; Deng, Y.; Liu, B.; Wan, H.; Gao, F.; Sun, K.; Dong, L. *J. Colloid Interface Sci.* **2011**, *355*, 464−471.
(31) Sánchez, M.; Chen, P.; Reinecke, T.; Muhler, M.; Xia, W. *ChemCatChem.* **2012**, *4*, 1997−2004.
(32) Choi, H.; Park, J. *J. Phys. Chem. B* **2005**, *109*, 4333−4340.
(33) Masa, J.; Zhao, A.; Xia, W.; Sun, Z.; Mei, B.; Muhler, M.; Schuhmann, W. *Electrochem. Commun.* **2013**, *34*, 113−116.
(34) Jagadeesh, R. V.; Surkus, A. E.; Junge, H.; Pohl, M. M.; Radnik, J.; Rabeah, J.; Huan, H.; Schunemann, V.; Bruckner, A.; Beller, M. *Science* **2013**, *342*, 1073−1076.
(35) Xiong, J.; Ding, Y.; Wang, T.; Yan, L.; Chen, W.; Zhu, H.; Lu, Y. *Catal. Lett.* **2005**, *102*, 265−269.
(36) Suzuki, K.; Kaneko, T.; Yoshida, H.; Morita, H.; Fujimori, H. *J. Alloys Compd.* **1995**, *224*, 232−236.
(37) Das, B.; Reddy, M. V.; Rao, G. V.; Chowdari, B. V. *J. Mater. Chem.* **2012**, *22*, 17505−17510.
(38) den Breejen, J. P.; Radstake, P. B.; Bezemer, G. L.; Bitter, J. H.; Froseth, V.; Holmen, A.; de Jong, K. P. *J. Am. Chem. Soc.* **2009**, *131*, 7197−7203.